ELSEVIER

Atmospheric Research 43 (1997) 277–295

ATMOSPHERIC RESEARCH

The effect on thunderstorm charging of the rate of rime accretion by graupel

I.M. Brooks [a,1], C.P.R. Saunders [a,*], R.P. Mitzeva [b], S.L. Peck [a]

[a] *Department of Physics, UMIST, Manchester M60 1QD, UK*
[b] *Faculty of Physics, University of Sofia, Sofia-1126, Bulgaria*

Abstract

Analysis of laboratory data concerning the charging of small graupel pellets in thunderstorms has shown that the charge transferred to a riming target during collisions with ice crystals is affected by the rate of rime accretion. Earlier, we found that the *magnitude* of the charges transferred depend on velocity; however, the velocity also controls the rate of target rime accretion which affects the *sign* of the charge transfer with higher accretion rates favoring positive rimers during crystal collisions. Experiments have now been conducted to confirm this effect and a set of equations are presented describing the charge transfer as a function of ice crystal size, velocity, temperature and rime accretion rate. As a first step in determining the importance of the new formulations on thunderstorm electrification, they have been tested in a one-dimensional numerical model. The model results indicate that the normal thunderstorm positive dipole can be generated in the observed time by means of ice crystal/graupel interactions. © 1997 Elsevier Science B.V.

1. Introduction

Laboratory measurements of the charges transferred between colliding ice crystals and riming ice particles, representing falling graupel pellets in thunderstorms, have shown that the sign and magnitude of the charges are dependent on the detailed cloud microphysical conditions and that such interactions may be responsible for thunderstorm electrification. Charge transfer experiments were reviewed by Saunders (1993) and studies of particular relevance to the current work are mentioned below. Reynolds et al.

* Corresponding author. Tel.: +44-161-2003909; fax: +44-161-2003941; e-mail: clive.saunders@umist.ac.uk.

[1] Now at Scripps Institution of Oceanography, University of California, San Diego, CA 92093-0221, USA.

PII S0169-8095(96)00043-9

(1957) were the first to note the requirement for liquid water to be present in order that the magnitude of the charges transferred during ice crystal collisions with a riming target be important to thunderstorm electrification. Takahashi (1978) found that the sign of the charge was controlled by both the cloud temperature and the liquid water content (LWC). Jayaratne et al. (1983) measured the dependence of the magnitude of charge transfer on velocity and crystal size and also noted that the charge sign depends on temperature and liquid water content; they suggested that the normal thunderstorm dipole is generated by the negative charging of graupel at low temperatures, the positive crystals being carried up in the updraught, and that at temperatures warmer than a certain critical value called the Reversal Temperature, positively charging graupel can fall to form a lower region of positive charge. Baker et al. (1987) proposed that the sign of the charge transfer is controlled by the difference in diffusional growth rates of the two interacting particles; the particle that grows faster charges positively: other possible charging mechanisms were discussed by Saunders (1994). Keith and Saunders (1990) extended the laboratory measurements to higher velocities and larger ice crystals (25 m s^{-1}, 800 μm). Saunders et al. (1991) — from now on, SKM — noted from the work of Jayaratne and Saunders (1985) and Baker et al. (1987), that the charge transfer process is influenced by the presence of accreted rime on the target and so in subsequent work, rather than use LWC as the controlling variable, they use the Effective Liquid Water Content, EW, which is that portion of the cloud LWC that is captured by the rimer by virtue of its collision efficiency; EW is thus dependent on droplet and collector sizes and their relative velocity. SKM quantified the charge transfer in terms of several variables (EW, temperature, relative crystal/graupel velocity, and crystal size), and presented equations from which charge transfer values could be obtained for inclusion in numerical models of the development of electric fields in thunderstorms. Fig. 1 summarizes their findings in which the charge sign dependence on EW and temperature is shown.

The charge transfer measurements have led to several calculations of the charging rate in thunderstorms based on the laboratory results (for example, Rawlins, 1982;

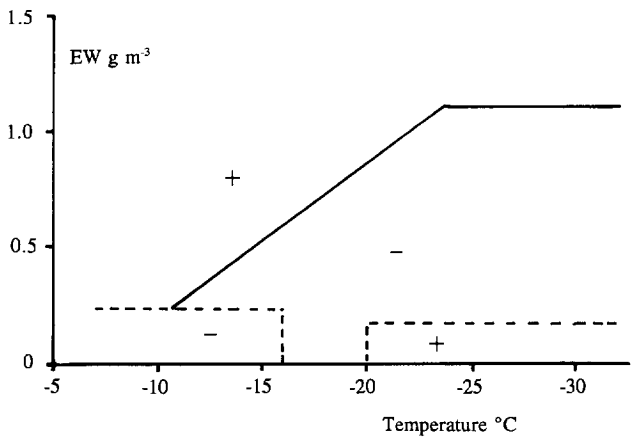

Fig. 1. The sign of the charge transfer to a riming target during ice crystal collisions at 3 m s^{-1} as a function of Effective Liquid Water Content and temperature. (From Saunders et al., 1991.)

Takahashi, 1984; Helsdon and Farley, 1987; Norville et al., 1991; Ziegler et al., 1991; and Scavuzzo and Caranti, 1996) which show that the ice crystal/graupel charging process can generate thunderstorm electric fields of the observed magnitude and growth rate (Krehbiel, 1986). Traditionally, numerical models have used values of LWC rather than EW, effectively assuming that EW = LWC, but this is certainly not true for small graupel falling at a few meters per second; furthermore, EW is the quantity determined in the laboratory analysis and so values of EW should be used in numerical models. For example, Fig. 1 shows that charge sign reversal at -15°C occurs for EW around 0.5 g m^{-3}; the LWC that this corresponds to in the cloud depends on the details of particle and droplet sizes and relative velocities. Recent calculations by Wojcik (1995) have used the SKM equations to calculate thunderstorm charging rates and have compared the effect of using LWC or EW values. Their model results using SKM (Fig. 1) with values of EW produced a more realistic charge distribution in the thunderstorm than the use of LWC values; essentially, the use of EW permits the continued negative charging of graupel at substantial values of LWC.

In much of the earlier work in Manchester, and in other groups, there has been an implicit assumption that the magnitude of the charge transfer is controlled by velocity, among other variables, but that the sign of the charge is independent of velocity; in particular, it has been assumed in model calculations that Fig. 1 is velocity independent. However, the rate of accretion of rime on the target is also velocity dependent and Brooks (1993) pointed out that increased rates of accretion are equivalent to an increase in EW which can favor positive rimer charging, as is clear from Fig. 1. Increasing either EW or velocity should therefore have a similar effect in their influence on the sign of the charge transfer. This hypothesis is examined here and leads to a revision of the charge transfer equations presented in SKM; the consequences of the new analysis to thunderstorm electrification are tested by means of a one dimensional model.

2. Discussion of the effect of velocity on rime accretion rate and charging

There are two effects of velocity on crystal/rimer charge transfer. (1) Increasing the velocity of impact of ice crystals on the rimer increases the charge transfer by virtue of the increased energy of collision; perhaps larger areas of the surface, deeper penetrations of the colliding particle or longer contact times are responsible for the increased charge transfer. (2) Increasing the impact velocity also increases the rate at which rime is accreted which itself affects the charge transfer through heat and vapour release from freezing droplets.

In previous studies of the dependence of charge transfer on crystal/rimer velocity by Keith and Saunders (1990), shown in Fig. 2, the liquid water content in the cloud was deliberately reduced when the speed was increased so that the rate of accretion of rime by the target was the same at all speeds. In this way the charge dependence on velocity was determined independently of the rate of rime accretion and this velocity dependence appears in the charge transfer equations in SKM and has been used in various model calculations of electric field growth rates in thunderstorms. The results of Fig. 2 show that a target charging with a particular sign at low speed continues to charge with the

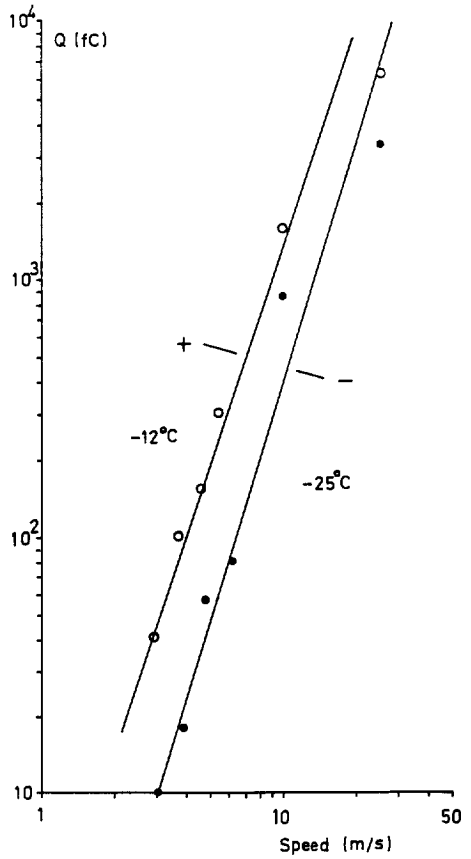

Fig. 2. The dependence of charge transfer (per crystal separation event) on velocity, for positive and negative rimer charging. The Rime Accretion Rate was constant at all velocities. (From Keith and Saunders, 1990).

same sign at speeds as high as 25 m s^{-1}. This observation led SKM to conclude that their results showing charge sign dependence on temperature and EW (Fig. 1) are independent of velocity. However, increased rime accretion favors positive rimers, a result noted before but in the context of experiments conducted at constant velocity. For example consider the negative charging zone in Fig. 1, and note the effect at constant temperature and velocity, 3 m s^{-1}, of an increase in EW achieved by increasing the LWC in the cloud; negative rimer charging may be reversed to positive at high EW.

The important parameter to consider here is the rime accretion rate, RAR, which combines the dependence on EW and velocity (RAR = EW $\times$ V, g m^{-2} s^{-1}). In particular, the hypothesis is illustrated by considering a point in Fig. 1 on the diagonal zero charge transfer line at a particular value of EW and corresponding temperature: increasing the velocity increases the RAR leading to positive charging; to obtain zero charging again, the RAR may be reduced by reducing the LWC in the cloud. Fig. 1 may be converted to account for the RAR dependence by replacing EW with EW $\times$ $V/3$ as

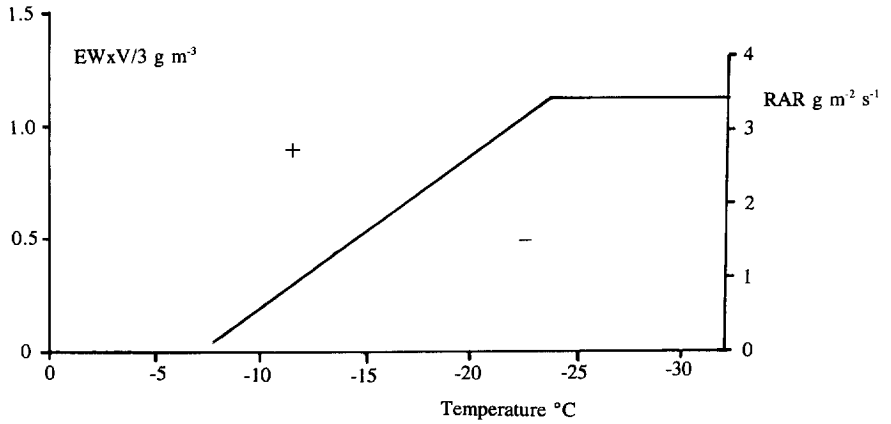

Fig. 3. The revised version of Fig. 1 taking into account the effect of Rime Accretion Rate and temperature on the sign of the charge transfer to the target.

shown in Fig. 3; the factor 3 appears because the SKM experiments were performed at 3 m s^{-1}. The low EW charging zones in Fig. 1 are not presented in Fig. 3 for reasons explained later. The charge transfer equations presented in SKM include values of EW, these too may be converted by replacing EW by EW $\times$ $V/3$ as shown below.

3. Experimental verification of the velocity effect

Experiments were conducted in the Manchester cloud chamber described previously by Keith and Saunders (1990). A supercooled water droplet cloud was formed and seeded to produce ice crystals in the usual way; the cloud was then drawn at a controllable velocity past a stationary 3 mm diameter metal rod target, representing a falling graupel pellet, mounted in a tube. The output from an amplifier connected to the target detected the charge transferred during ice crystal interactions with the riming target. The effective liquid water content in the cloud, EW, was determined for the period of experimental interest by drawing cloud at the same velocity past a similar riming target sampling the same cloud and by weighing the accreted rime after each run. Droplet and ice crystal spectra could be obtained from microscopic analysis of formvar replicas obtained by drawing cloud past a formvar coated slide in a separate tube connected to the chamber. The temperature within the cloud chamber was monitored by thermocouples.

One of the objectives of these experiments was to compare charge transfers at 3 m s^{-1} with those at 9 m s^{-1} in order to help resolve differences between the laboratory results obtained in Manchester with those of Takahashi (1978) who used only the higher speed and who noted charge sign reversal from negative to positive at higher values of LWC than reported in Manchester. Subsequent work by Brooks and Saunders (1995) has linked this discrepancy with the measurements of LWC in the 1978 experiments and will be discussed later.

Table 1
Approximate values of the critical effective liquid water content and rime accretion rate at the charge sign reversal points for two crystal/graupel velocities

T (°C)	V (m s^{-1})	EW (g m^{-3})	RAR = EW × V
−15	9	0.2	1.8
	3	0.6	1.8

Experiments were carried out to determine the critical value of EW at which the charge transfer reverses sign at velocities of 3 and 9 m s^{-1}. The continuously supplied supercooled water droplet cloud was seeded briefly in the lower cloud chamber by a nitrogen cooled rod after which the ice crystals grew in the cloud; one minute after seeding, formvar replicas show droplets in the diameter range 6 to 24 μm with crystals from 22 to 100 μm. In these experiments, riming of the targets was started 1 min after seeding and continued for 1 min. The sign of the charging current to the target was determined during the latter half of this period when the riming conditions had become steady. Successive experiments at decreasing values of EW were performed at a fixed temperature and velocity by adjusting the LWC in the cloud. At high EW the target charged positively; at low EW it charged negatively and the critical value for charge sign reversal was noted. Table 1 gives details of the effective liquid water contents for charge reversal in two experiments at 3 and 9 m s^{-1} at a temperature of −15°C. Also shown is the critical rime accretion rate at each velocity. Similar experiments were performed at −10°C and −15°C at speeds of 6 and 10 m s^{-1}; as in Table 1 the critical values of RAR proved to be independent of velocity. Several experiments were also performed at −15°C at a range of velocities and the average RAR for charge sign reversal was at RAR = 1.7, in fair agreement with Fig. 3.

Further experiments were carried out to confirm the dependence of charge sign on velocity under constant ambient conditions at a temperature of −15°C and liquid water content just below 0.5 g m^{-3}; the results are shown in Fig. 4. Airflow past the target was started about 90 s after seeding the cloud; the initial charge transfers are variable because the cloud conditions are still changing rapidly due to competition for the available vapour by the growing ice crystals, but conditions become more stable later in the run when the sign of the charge transfer to the target is seen to be velocity dependent. For velocities of 3 and 4.6 m s^{-1}, the rimer charges negatively, while at 6.3 and 7.7 m s^{-1}, the charging is positive. When the velocity changes, EW also changes because the droplet collision efficiency is velocity dependent. A charge sign reversal between 5 and 6 m s^{-1}, from Fig. 4, with an EW around 0.3 appropriate for the droplet spectrum used, leads to a RAR of around 1.7 which is in fair agreement with Fig. 3 at −15°C. Thus, Fig. 4 is further confirmation of the controlling influence of RAR on the sign of rimer charging.

The results shown in Table 1 show that higher effective liquid water contents are required to achieve charge reversal at 3 m s^{-1} than at 9 m s^{-1} and that the rime accretion rate maintains a constant value at the charge sign reversal point independent of velocity. Thus, with increase in speed, the diagonal charge sign reversal line in Fig. 1 moves to lower values of EW. The consequence of this result to thunderstorm electrifi-

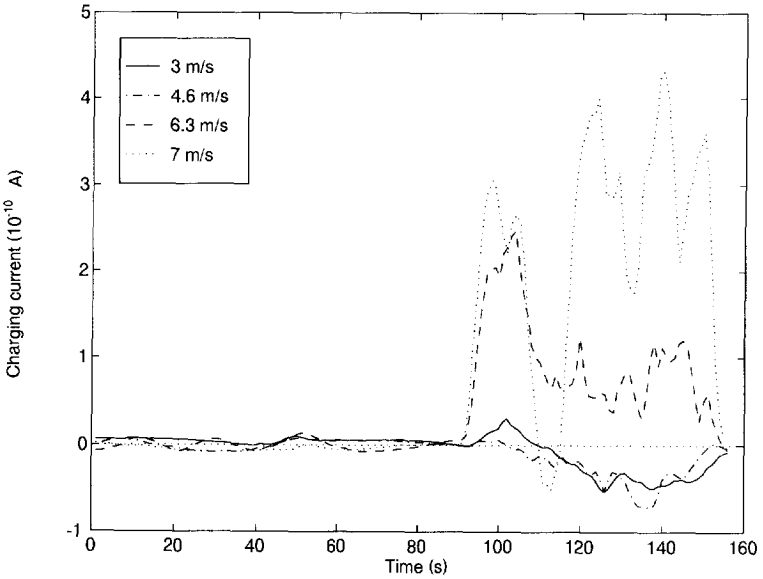

Fig. 4. The charging current to the riming target due to ice crystal collisions at a range of velocities.

cation may be that large graupel falling at several meters per second with a high droplet collision efficiency will be able to charge negatively only in regions of cloud with low EW. On the other hand, small graupel falling at velocities less than 3 m s^{-1} will charge negatively at higher values of EW than indicated in Fig. 1. Charge sign reversal at lower EW with higher speeds as noted here does not help account for the high values of LWC for charge sign reversal at 9 m s^{-1} reported by Takahashi (1978). The first of these issues is studied in a numerical model of charge generation in thunderstorms that uses the revised charge transfer formulations shown below, and the second is considered in the discussion section.

4. The revised charge transfer equations

The charge transfer (Q, fC) to a riming target per ice crystal separation event is given in SKM:

$$Q = Bd^a V^b q \tag{1}$$

where d is the crystal size (m), V the speed (m s^{-1}), and q (fC) is determined from experimentally derived equations linking EW and T for the positive and negative charging cases. The constants B, a and b are given in Table 2 in SKM and in revised form as Table 2 here.

The revised equations presented here take account of the velocity dependence of the rime accretion by using RAR (EW $\times$ V) and also include some changes to the ranges of validity in order to overcome ambiguities in the data set. Figs. 3 and 5 in SKM and Fig.

Table 2
Values of the constants B, a and b in Eq. (1)

Charge sign	Crystal size (μm)	B	a	b
$+Q$	<155	4.9×10^{13}	3.76	2.5
$+Q$	155–452	4×10^{6}	1.9	2.5
$+Q$	>452	52.8	0.44	2.5
$-Q$	<253	5.24×10^{8}	2.54	2.8
$-Q$	>253	24	0.5	2.8

3 here are relevant to the setting of appropriate ranges of applicability of the following equations. Data are not available above -7.4°C due to the experimental difficulties in controlling the cloud parameters at high temperatures; it is known that both positive and negative rimer charging can occur at temperatures above -7.4°C as a function of RAR, and further work is underway. Below -23.8°C, all positive charging is treated as if the temperature was -23.8°C because of the need to keep $(\mathrm{EW}\times V/3)<1.1$ for the negative charging case as can be seen from the horizontal portion of the critical line in Fig. 3. Within the limits of accuracy of the experimental measurements in SKM, negative charging was found to be independent of temperature. The equations are presented in two forms, involving EW or RAR; the factor 3 effectively normalizes the results of SKM which were obtained at 3 m s^{-1}.

For positive charging; $T<-7.4$°C,

$$q=20.22\times(\mathrm{EW}\times V/3)-1.36\times(-T)+10.05, \tag{2a}$$

$$q=6.74\times\mathrm{RAR}-1.36\times(-T)+10.05. \tag{2b}$$

For negative charging; $0.1<(\mathrm{EW}\times V/3)<1.1$,

$$q=3.02-31.76\times(\mathrm{EW}\times V/3)+26.53\times(\mathrm{EW}\times V/3)^{2}, \tag{3a}$$

$$q=3.02-10.59\times\mathrm{RAR}+2.95\times\mathrm{RAR}^{2}. \tag{3b}$$

In order to decide between the use of Eqs. (2a), (2b), (3a) and (3b), Eqs. (4a) and (4b), representing the diagonal line in Fig. 3, provide critical values of EW and RAR as a function of temperature.

$$\mathrm{CEW}\times V/3=-0.49+6.64\times10^{-2}\times(-T)\ (\mathrm{g\ m^{-2}\ s^{-1}}), \tag{4a}$$

$$\mathrm{CRAR}=-1.47+0.2\times(-T)\ (\mathrm{g\ m^{-2}\ s^{-1}}). \tag{4b}$$

A one dimensional numerical model has been used as a first step in checking the consequences of this new charge transfer dependence on rime accretion rate to the development of the charge dipole during the electrification of a typical thunderstorm.

5. The numerical model

The one dimensional numerical cloud model includes parameterization of the ice crystal/graupel charging mechanism. According to the model, convective clouds are composed of active and non-active cloud masses (Andreev et al., 1979a) and it is assumed that the active mass is formed by successive ascending spherical thermals while the non-active cloud region is formed by thermals that have previously risen and stopped at their convective levels. The non-active cloud mass expands and the temperature excess, water vapour, cloud droplets, and ice crystals in this region vary in time because of turbulent diffusion and evaporation (Andreev et al., 1979b). The ascending thermals entrain air from a cloudless environment or from a non-active cloud region depending on their position.

The thermals are driven by the buoyancy force reduced by entrainment and the weight of the hydrometeors present. The vertical temperature structure takes into account cooling as the thermals ascend, entrainment of environmental air and heat released by the microphysical processes which are represented using a bulk parameterization scheme similar to that described by Andreev (1976). Four categories of hydrometeor are taken into account in the moving thermals: cloud and rain drops, ice crystals and graupel. The cloud droplets are formed by condensation; rain drops form by autoconversion of the cloud droplets and grow by collision and coalescence with cloud drops (Kessler, 1969). Ice crystals originate by the activation of ice nuclei in supercooled cloud droplets, their concentration being given by Fletcher (1962). Homogeneous freezing occurs below $-40°C$. Graupel forms by the freezing of rain drops (Bigg, 1953), contact nucleation of ice crystals and rain droplets (Cotton, 1972) and conversion of ice crystals (Hsie et al., 1980). Ice crystals grow by deposition and by riming. Hail grows by deposition and coalescence with cloud and rain drops (Wisner et al., 1972). The values of EW are determined from the LWC, taking into account the droplet and graupel sizes and relative speeds using the collision efficiency formulation of Fonda and Herne (1957). Evaporation of rain drops and melting of graupel during their descent (Farley and Orville, 1986) as well as recycling, is included. The cloud drops and ice crystals are assumed to be monodisperse and have negligible fall velocities and so move upward with the air. A Marshall–Palmer type distribution is used for the rain drops and graupel (see Marshall and Palmer, 1948). Precipitation fallout is calculated in the same manner as in Cotton (1972) and comprises those precipitation drops and graupel with terminal velocities greater than the updraught velocity.

For the purposes of modelling cloud electrification the following assumptions are made. Charge is generated by the rebounding collisions of ice crystals and graupel. The sign and magnitude of the charge per crystal separation event depends on the crystal size, the impact velocity, and the rime accretion rate as defined in the equations presented above. From Keith and Saunders (1989), typically 30% of the ice crystals in the path of the rimer rebound from the graupel and so are involved in charge transfer. The charging rate per unit volume of model cloud is calculated as in Mitzeva and Saunders (1990) using Eq. (1) with values of a and b from Table 2. Ice crystals and graupel in the ascending thermals as well as falling graupel are the charge carriers. Graupel production by drop capture of crystals and by autoconversion conserves the

(average) charge on the crystals (from earlier interactions) when it becomes the initial graupel charge and is added to the total graupel charge density. The reduction of charge density in ascending thermals due to entrainment is taken into account. The net charge density in ascending thermals is established by summing the charges on the ice crystals and ascending graupel. The net charge density in the non-active part of the cloud is the sum of the charge on falling graupel and the ice crystals present. The charges on the ice crystals and graupel do not affect the cloud microphysics and dynamics.

The differential equations, describing the dynamical, microphysical and electrical processes in the ascending thermals are integrated numerically by the Runge–Kutta method. The calculations are carried out for thermals ascending from cloud base to the height of zero velocity. The numerical integration of the equations, describing the changes with time of the characteristics of the nonactive cloud region, begins after one of the ascending thermals stops at its convective level. The calculated temperature, vapour mixing ratio, and cloud liquid and ice mixing ratios of the diffusing thermals are used in the estimation of the environmental conditions of the ascending thermals. The masses of the raindrops and graupel falling out of the ascending thermals are calculated at each integration step. Their terminal fall speed depends on their mass-median diameter, which changes because of melting and evaporation. During the descent, graupel particles charge by rebounding collisions with ice crystals in the non-active cloud mass or in the ascending thermals.

6. The case study

The model has been run using the environmental conditions observed on July 19, 1981 during the CCOPE experiment near Miles City, Montana. This case was chosen for the simulation because it involved an isolated small cumulus cloud appropriate for the model described above. Moreover, many field measurements of the microphysical, dynamical and electrical properties of this cloud have been reported (Gardiner et al., 1985; Dye et al., 1986) and the same cloud has been used in other numerical simulations (Helsdon and Farley, 1987; Norville et al., 1991). The numerical experiments in Mitzeva and Andreev (1984) showed that various types of convective clouds with different cloud top heights and life times may be formed depending on the initial parameters chosen. From the observations of Dye et al. (1986), the cloud base was at 3.9 km above mean sea level (MSL) at 0.8°C to 1.1°C. The updraught speed at cloud base was between 1 and 5 m s^{-1} and the cloud was 2 to 3 km wide. In accordance with these observations the following model parameters were used: cloud base height 3.9 km, initial thermal radius 2 km, initial vertical velocity at cloud base 3 m s^{-1} and temperature at cloud base 1°C. The time interval between the ascent of thermals from cloud base was set arbitrarily at 2 min. The turbulent diffusion coefficient for the non active cloud mass is taken as 200 m^2 s^{-1} which is a value based on observations (Shmeter, 1987) and is an average taken over the range of clouds of this type. Eight thermals were used for the simulation. Using the above parameters, the model cloud top height increased from 7.5 km at 17 min to 11.6 km MSL at 24 min, which is about 1 km higher than the observed cloud top height. A comparison by Mitzeva (1988) showed that this model simulates approxi-

mately the dynamics and microphysics of the 19 July 1981 CCOPE case, although the model cloud grows a little faster than the CCOPE cloud, so it can be used as a first test of the revised laboratory analysis. In particular, 17 min model time corresponds approximately to the time 1622 shown in Fig. 3 of Dye et al. (1986). The maximum LWC in the model cloud is 1.4 g m^{-3} at 5.8 km MSL, while the measured maximum LWC is 2.5 g m^{-3} at 7 km MSL. The maximum updraught velocity in the model cloud is 17 m s^{-1} which is close to the observations (10 to 15 m s^{-1}).

7. Results of the model calculations

Fig. 5 shows the evolution of charge in the ascending thermals; the total charge is negative in the temperature region −10 to −30°C with a maximum around −20°C at 18.5 min; later, a positive region develops at temperatures below −30°C with maximum charge densities respectively of −2.8 and 3.2 nC m^{-3}. Fig. 6 shows the charge densities in the non active part of the model cloud and the charge on graupel in the downdraught as a function of cloud temperature and model time. The charge density is positive in regions with temperatures above −17°C at around 18 min; these positively charged particles fall to form the positive region at 19 min at temperatures above −10°C and then continue to fall while a negative center develops around −14°C at 19 min. Since the model is composed of active (ascending thermals), non active cloud regions and precipitating graupel, the overall location of the negative and positive charges in the model cloud comes from a combination of Figs. 5 and 6.

The results show that in the initial stage of cloud electrification (17–19.5 min) the lower part of the model cloud (temperatures above −17°C) is charged positively and the

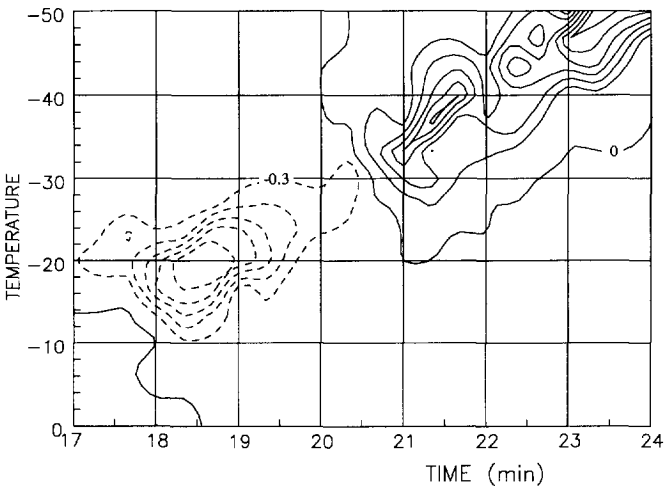

Fig. 5. The total charge density in nC m^{-3} in ascending thermals as a function of cloud temperature and model time. Contour interval is 0.5 nC m^{-3} and the maximum positive value is 3.2 nC m^{-3} and the maximum negative value is −2.8 nC m^{-3}. (Negative charge, dashed lines; positive charge, solid lines).

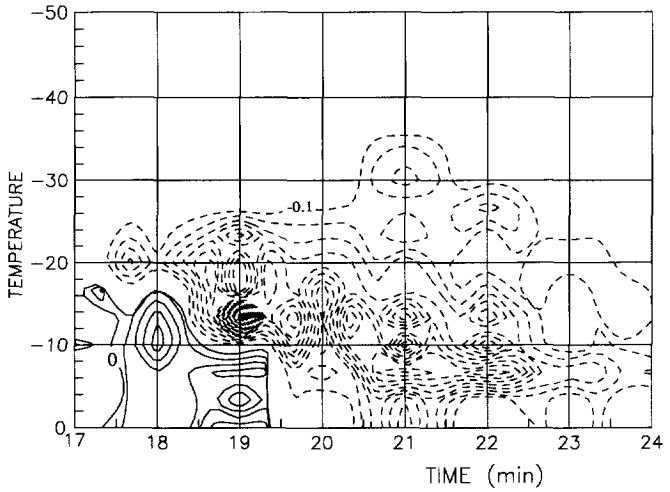

Fig. 6. The total charge density in the non-active cloud region in nC m^{-3} as a function of cloud temperature and model time. Contour interval for positive charge (solid lines) is 0.001 nC m^{-3} and for negative charge is 0.1 nC m^{-3} (dashed lines). The maximum positive value is 0.005 nC m^{-3} and the maximum negative value is -1.8 nC m^{-3}.

upper part (-17 to -25°C) is charged negatively leading to a weak 'inverted' dipole. This result is expected at this time because graupel charge positively when the particle interaction region is situated below the charge sign reversal level. The positively charged graupel fall and become widely distributed below the negative region.

Figs. 5 and 6 show the two charge distributions from 20 to 24 min towards the end of

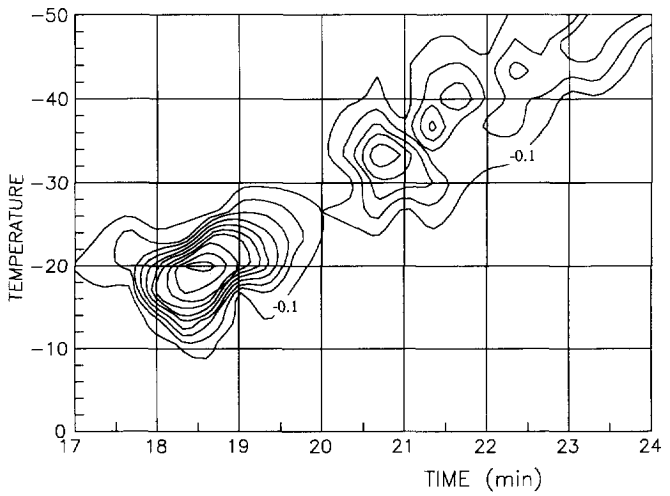

Fig. 7. The negative charge density in nC m^{-3} on graupel in ascending thermals as a function of cloud temperature and model time. The contour interval is 0.2 nC m^{-3} and the maximum value is -2 nC m^{-3}.

the growth phase of the storm when the lower part of the model cloud is charged negatively and the upper part positively, which gives a 'normal' thunderstorm dipole orientation in agreement with the observations of Gardiner et al. (1985) and Dye et al. (1986). Here, graupel are charging negatively above the charge sign reversal level. Fig. 7 represents the negative charge carried by graupel in the ascending thermals; comparison between Figs. 5 and 7 shows that during the 17 to 24 min period at temperatures below −10°C, graupel are the main carriers of negative charge in ascending thermals. Fig. 8a shows that between 17 and 21 min at temperatures between −10 and −30°C

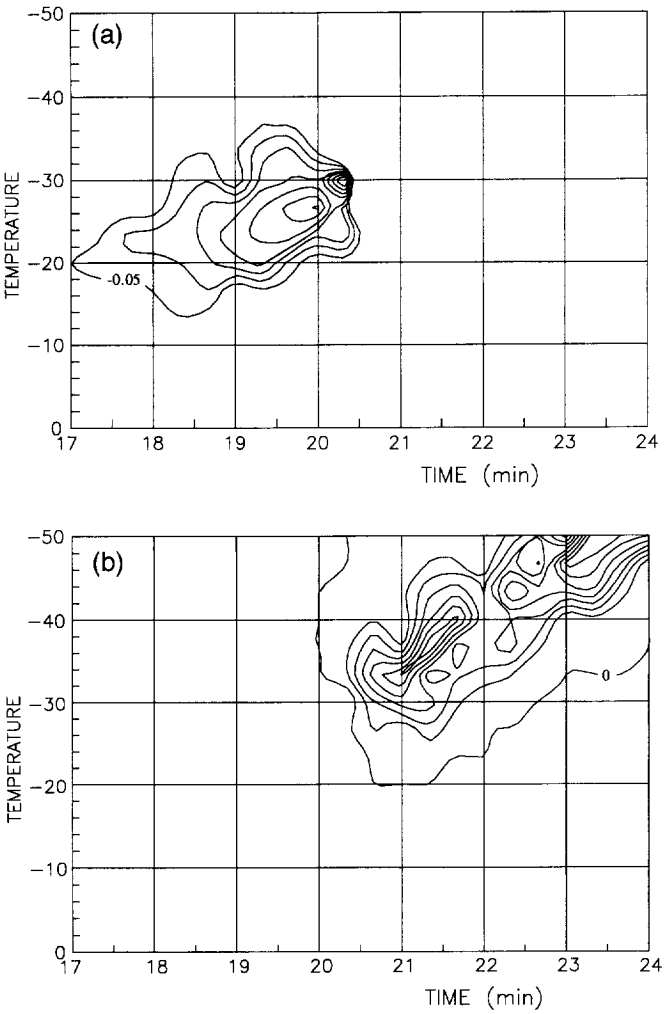

Fig. 8. (a) The negative charge density in nC m^{-3} on ice crystals in ascending thermals as a function of cloud temperature and model time. The contour interval is 0.05 nC m^{-3}. (b) The positive charge density in nC m^{-3} due to ice crystals in ascending thermals as a function of cloud temperature and model time. The contour interval is 0.5 nC m^{-3}.

there are also negatively charged crystals in the ascending thermals because the crystals that were charged negatively at temperatures warmer than the Reversal Temperature in the lower part of the cloud have been carried aloft. Thus, in this part of the model cloud, in this period of time, both graupel and ice crystals contribute to the negative charge density as postulated by Jayaratne et al. (1983). The magnitude of the positive charge carried by crystals between 20 and 24 min at low temperatures, as shown in Fig. 8b, confirms that ice crystals were the carriers of positive charge in the ascending thermals, in agreement with many field observations of positively charged crystals in thunderstorm anvils.

Analysis of the charge distribution in Fig. 6 shows that the net charge density is due mainly to the graupel falling out of the ascending thermals. The small (< 0.005 nC m^{-3}) positive charge density in the environment between 17 and 19 min is due to those graupel charged positively during interactions with crystals in the ascending thermals at temperatures higher than the reversal temperature that have precipitated out. The negative charge in the non active part of the cloud between 20 and 24 min is also due to precipitating graupel which were charged negatively in the region of cloud colder than the reversal temperature. The results show that although the magnitude of the negative charge carried on falling graupel decreases when they enter the region with temperatures higher than the reversal value, there is not enough time for the sign of their charge to change, which again is in agreement with the time scale of electric charge separation observed in the CCOPE cloud as shown in Fig. 13 of Dye et al. (1986).

8. Discussion

The laboratory experiments show that there is a difference between charge transfer measurements conducted at constant effective liquid water content and those at a constant rime accretion rate, confirming that RAR has an important influence on rimer charge sign. The charge sign boundaries in Fig. 1 move to lower effective liquid water contents as velocity increases; the figure can be redrawn with RAR as the ordinate, as in Fig. 3, when it becomes valid over a range of graupel fall velocities. The dependence of charge sign on velocity has not previously been noted because studies into the effect of velocity on the charging process have tended to work either deep into the positive and negative charging zones (Jayaratne et al., 1983 and SKM) or at a constant rime accretion rate (Keith and Saunders, 1990).

The result that both EW and V, through the RAR, influence the sign of the charge transfer might suggest that the latent heat released by the freezing droplets increases the rimer temperature and controls the charge transfer. However, temperature differences between the interacting particles have been ruled out as the driving mechanism of charge transfer (Gaskell and Illingworth, 1980, and Jayaratne et al., 1983). Furthermore, increased riming leading to a surface temperature increase both strengthens negative charging (at least at low EW) in the negative rimer regime and increases positive charging in the positive regime. So, it seems likely that the influence of riming on charging is directly associated with the presence of liquid water on the rimer surface as measured by the RAR as this can be increased with equal effect by an increase in

velocity or EW. The effect of the captured droplets freezing at 0°C is to provide vapour to the surrounding, colder, rimer surface and to provide heat that increases the average surface temperature which, in turn, reduces vapour deposition from the environment. In this way the sign of the rimer charging is controlled by the relative diffusional growth rates of the interacting particles, Baker et al. (1987), and by the nature of the quasi-liquid surface layer as discussed by Baker and Dash (1994). At high temperatures, with relatively long droplet freezing times and correspondingly long periods of vapour release, or with high EW, the rimer charges positively because its surface is bathed in vapour, and so it has more vapour available to it than the ice crystals. At low temperatures, and relatively short droplet freezing times with a consequent brief vapour release, or with low EW, the heat released to the rimer reduces diffusional growth below that of the ice crystals and it charges negatively. Saunders and Brooks (1992) showed that a riming target experiencing ice crystal collisions charges positively or negatively independently of whether the riming surface is growing by vapour diffusion or sublimating; the relative growth rates of the interacting ice particles appears to control the sign of the charge transfer. Other factors related to the velocity may also affect the charging; ventilation of the target increases with velocity which affects the heat balance of the rime; the distribution of droplet sizes collected by the rimer changes because the collection efficiencies of the droplets increase with velocity, which may make a significant difference to the density and structure of the rime and to the pattern of vapour deposition around freezing droplets which in turn influences the charge transfer. On the other hand, the absence of sign reversal with increased velocity at constant RAR shown in Fig. 2 suggests that rime density, which increases with velocity, does not play a major role in influencing the sign or magnitude of the charge transfer. A determination of the extent to which the factors mentioned above actually affect the charging behavior of a rimer, particularly in the context of the charge sign dependence on the relative growth rates of the interacting particles, awaits detailed modelling studies of heat and vapour fluxes on a riming surface, and experimental work with carefully controlled and monitored cloud conditions involving a variety of well categorized droplet spectra.

Fig. 1, from SKM, shows positive and negative zones of charging at low EW. When the effect of these zones was tested in the same numerical model described here using the equations in SKM, the zones were not found to influence the cloud electrification in a significant way. They have not been included in the new formulation involving RAR for this reason and because it is experimentally difficult to verify the charge sign dependence on RAR at such low values of EW. For example, a test in which RAR was kept constant at a charge sign reversal point in Fig. 1 would involve increasing the velocity and decreasing EW to values that have been found hard to control in the cloud chamber. Alternatively, EW could be increased and velocity decreased to keep RAR constant, however, measurement of the small charge transfers that occur at low crystal impact velocities is impossible because of the small signal to noise ratio.

In experiments with ice crystal/rimer collisions at 9 m s^{-1}, Takahashi (1978) noted rimer charge sign reversal from negative to positive with increase in LWC; for example at -15°C reversal occurred at a LWC of 3.5 g m^{-3}; reversal in the Manchester studies occurs at considerably lower LWC. The present work has shown that the required LWC for charge sign reversal decreases with increase in velocity due to increased rime

accretion, apparently making reconciliation with the data of Takahashi more difficult. However, the analysis below shows that the differences between the two sets of measurements may be brought closer together by accounting for ice crystal capture on the LWC probe and the reduction in droplet sizes in the Takahashi investigation. Recent work by Brooks and Saunders (1995) has shown that in the 1978 study, the ice crystal continuous nucleation technique used could have produced overestimated values of LWC in the laboratory cloud because the rimer collected both droplets and ice crystals and the total deposit was weighed in the determination of LWC. The 1978 experiment was replicated by Brooks (1993) and Brooks and Saunders (1995) with 4 mm diameter rod targets rotating at 9 m s^{-1} in a continuously seeded cloud. The LWC was determined in 1978 by weighing a target moving round in the cloud, and then accounting for the droplet collision efficiency of 80%, a figure applicable to the initial droplet spectrum before seeding the cloud, so that the reported LWC of 3.5 g m^{-3} for charge reversal at -15°C indicates measured accretion on the target equivalent to 2.8 g m^{-3}. Brooks and Saunders used formvar coated slides, past which the cloud was drawn, to provide values of the relative masses of droplets and ice crystals in a continuously seeded cloud; the droplet mass typically was only 13% of the total cloud mass. Thus the collected 'LWC' of 2.8 g m^{-3} indicates a droplet collection by the target equivalent to 0.36 g m^{-3}, which is the effective LWC (EW). The droplet spectrum in the seeded cloud in the 1978 work is not known (a histogram of droplet data for an unseeded cloud is provided but droplet sizes can decrease substantially in a seeded cloud); in a simulation using the same continuous cloud nucleation technique, the seeded cloud droplet spectrum extends from 4 to 9 μm peaking at 5 μm (Brooks and Saunders, Fig. 4); this spectrum involves much smaller droplets than are usually used in the Manchester work. Using droplet collision efficiencies according to Langmuir and Blodgett (1946) for the small droplet spectrum with a 4 mm target at 9 m s^{-1}, the weighted collision efficiency is 21%. Thus an estimate, from our simulations of the 1978 experiments, of the critical LWC in that cloud for charge sign reversal at -15°C, is 1.7 g m^{-3} (0.36/0.21) which can be compared with the value in the 1978 paper of 3.5 g m^{-3}. The corresponding critical RAR in the 1978 work is 3.2 g m^{-2} s^{-1} (0.36×9) which can be compared with the present value of 1.5 g m^{-2} s^{-1} shown in Fig. 3 at -15°C. Thus by accounting for the over estimation of LWC in the 1978 experiments, then converting the LWC through the effective liquid water to the Rime Accretion Rate, the results of the 1978 work and the Manchester experiments, as far as results below -10°C are concerned, have been brought closer together. In particular, it is possible that Takahashi's results apply to a smaller droplet size spectrum than is usually used in the Manchester experiments.

9. Conclusion

The effect on graupel/crystal charge transfer of increased rime accretion rate with velocity has been tested and the equivalence of increase in velocity or effective liquid water content has been confirmed. The combined effect is represented by the rime accretion rate ($RAR = EW \times V$) and has been included in the previously published

charge transfer equations by normalizing them by multiplying EW by $V/3$, the earlier experiments being performed at 3 m s^{-1}. The revised equations are presented here and the consequences of the new formulations have been tested in a numerical thundercloud electrification model. The model results using the revised equations for the dependence of the magnitude and sign of charge transfer due to rebounding ice crystal collisions on RAR, show that a negative charge region is developed between -10 and -30°C during the early growth stage of the cloud, which corresponds to real cloud observations. The main carriers of negative charge in this temperature region are graupel; the ice crystals have only a small contribution to the negative charge during this short period of time. When the intensification of cloud charging begins, the positive charge in the model cloud is carried by ice crystals and is located in the upper part of the cloud while the negative charge is carried on graupel in the downdraughts. These results using a simple model need further investigation using three dimensional models, but the preliminary results from the present work indicate agreement with field measurements and show that the critical charge sign reversal temperature and charge transfer magnitude dependence on RAR rather than on EW alone can lead to realistic electric field generation in thunderstorms.

Acknowledgements

This work is supported by the Natural Environment Research Council, the Royal Society and the National Science Foundation in Bulgaria under grant NZ-41-91.

References

Andreev, V., 1976. Microphysical effects of a dynamical model of an active isolated element of convection. Bulg. Geophys. J., 4: 17–27.

Andreev, V., Syrakov, D. and Mitzeva, R.P., 1979a. Modelling of convective cloud formation as successive ascending thermals. Bulg. Geophys. J., 1: 3–9.

Andreev, V., Syrakov, D. and Mitzeva, R.P., 1979b. Turbulent diffusion of a stopped unactive cloud thermal – A numerical experiment. Bulg. Geophys. J., 3: 3–8.

Baker, M.B. and Dash, J.G., 1994. Mechanism of charge transfer between colliding ice particles in thunderstorms. J. Geophys. Res., 99: 10621–10626.

Baker, B., Baker, M.B., Jayaratne, E.R., Latham, J. and Saunders, C.P.R., 1987. The influence of diffusional growth rate on the charge transfer accompanying rebounding collisions between ice crystals and hailstones. Q.J.R. Meteorol. Soc., 113: 1193–1215.

Bigg, E.K., 1953. The supercooling of water. Proc. Roy. Soc., London, B66: 688–694.

Brooks, I.M., 1993. Laboratory studies of thunderstorm charging processes. PhD Thesis, Manchester, UK.

Brooks, I.M. and Saunders, C.P.R., 1995. Thunderstorm Charging: Laboratory experiments clarified. Atmos. Res., 39: 263–273.

Cotton, W., 1972. Numerical simulation of precipitation development in supercooled cumuli – Part II. Mon. Wea. Rev., 100: 764–784.

Dye, J., Jones, J., Winn, P., Cerni, A., Gardiner, B., Lamb, D., Pitter, L., Hallett, J. and Saunders, C.P.R., 1986. Early electrification and precipitation development in a small isolated Montana thunderstorm. J. Geophys. Res., 91: 1231–1247.

Farley, R.D. and Orville, H.D., 1986. Numerical modelling of hailstones and hailstone growth, I, Preliminary model verification and sensitivity tests. J. Clim. Appl. Meteorol., 25: 2014–2036.

Fletcher, N.H., 1962. The Physics of Rainclouds, Camb. Univ. Press.
Fonda, A. and Herne, H., 1957. Hydrodynamic capture of particles by spheres, Mining Res. Establ. Rep. 2086, UK National Coal Board, Scientific Dept.
Gardiner, B., Lamb, D., Pitter, R.L, and Hallett, J., 1985. Measurements of initial potential gradient and particle charges in a mountain summer thunderstorm. J. Geophys. Res., 90: 6079–6086.
Gaskell, W. and Illingworth, A.J.I., 1980. Charge transfer accompanying individual collisions between ice particles and its role in thunderstorm electrification, Q.J.R. Meteorol. Soc., 106: 841–854.
Helsdon, J.H., and Farley, R.D., 1987. A numerical modeling study of a Montana thunderstorm; 2. Model results versus observations involving electrical aspects, J. Geophys. Res., 92: 5661–5675.
Hsie, E., Farley, R.D. and Orville, H., 1980. Numerical simulation of ice-phase convective cloud seeding. J. Appl., Meteorol., 19: 950–977.
Jayaratne, E.R., Saunders, C.P.R. and Hallett, J., 1983. Laboratory studies of the charging of soft-hail during ice crystal interactions, Q.J.R. Meteorol. Soc., 109: 609–630.
Jayaratne, E.R. and Saunders, C.P.R., 1985. Thunderstorm electrification: The effect of cloud droplets. J. Geophys. Res., 90: 13063–13066.
Kessler, E., 1969. On the distribution and continuity of water substance in atmospheric circulations. Meteor. Monr., Boston, 10: 1–84.
Keith, W.D. and Saunders, C.P.R., 1989. The collection efficiency of a cylindrical target for ice crystals. Atmos. Res., 23: 83–95.
Keith, W.D. and Saunders, C.P.R., 1990. Further laboratory studies of the charging of graupel during ice crystal interactions. Atmos. Res., 25: 445–464.
Krehbiel, P.R., 1986. The electrical structure of thunderstorms. The Earth's Electrical Environment, Studies in Geophysics. National Academy Press, pp. 90–113.
Langmuir, I. and Blodgett, K.B., 1946. A mathematical investigation of water droplet trajectories. Rep. No. 5418, US Army, Dayton, OH.
Marshall, J.S. and Palmer, W. McK., 1948. The distribution of raindrops with size. J. Meteorol., 5: 165.
Mitzeva, R.P., 1988. One dimensional cloud model as a succession of thermals. Simulation of the 19 July 1981 CCOPE case. Rep. of the 2nd Int. Cloud Modelling Workshop, Toulouse, France. WMO/TD No. 268: 195–200.
Mitzeva, R.P., and Andreev, V., 1984. Numerical experiments with the model of a convective cloud as a succession of thermals. Bulg. Geophys. J. 3: 14–22.
Mitzeva, R.P. and Saunders, C.P.R., 1990. Thunderstorm charging: calculations of the effect of the ice crystal size and graupel velocity. J. Atmos. Terr. Phys. 52: 241–245.
Norville, K., Baker, M. and Latham, J., 1991. A numerical study of thunderstorm electrification: Model development and case study. J. Geophys. Res., 96: 7463–7481.
Rawlins, F., 1982. A numerical study of thunderstorm electrification using a three dimensional model incorporating the ice phase. Q.J.R. Meteorol. Soc., 108: 779–800.
Reynolds, S.E., Brook, M. and Gourley, M.F., 1957. Thunderstorm charge separation, J. Meteorol., 14: 426–437.
Saunders, C.P.R., Keith, W.D. and Mitzeva, R.P., 1991. The effect of liquid water on thunderstorm charging, J. Geophys. Res., 96: 11007–11017.
Saunders, C.P.R. and Brooks, I.M., 1992. The effects of high liquid water content on thunderstorm charging. J. Geophys. Res., 97: 14671–14676.
Saunders, C.P.R., 1993. A review of thunderstorm electrification processes, J. Appl. Met., 32: 642–655.
Saunders, C.P.R., 1994. Thunderstorm electrification experiments and charging mechanisms. J. Geophys. Res., 99: 10773–10779.
Scavuzzo, C.M. and Caranti, G.M., 1996. Thundercloud electrification analysis: the dependence on the temperature–LWC diagram. J. Atmos. Sci., 53: 349–358.
Shmeter, S.M., 1987. Thermodynamics and Physics of Convective Clouds. Leningrad, p. 139.
Takahashi, T., 1978. Riming electrification as a charge generation mechanism in thunderstorms. J. Atmos. Sci., 35: 1536–1548.
Takahashi, T., 1984. Thunderstorm electrification – A numerical study. J. Atmos. Sci., 41: 2541–2558.
Wisner, C., Orville, H.D. and Myers, C., 1972. A numerical model of a hail bearing cloud. J. Atmos. Sci., 29: 1160–1181.

Wojcik, W.A., 1995. An examination of thunderstorm charging mechanisms using the IAS 2D storm electrification model. PhD thesis, South Dakota School of Mines, USA.

Ziegler, C.L., MacGorman, D.R., Dye, J.D. and Ray, P.S., 1991. A model evaluation of non-inductive graupel-ice charging in the early electrification of a mountain thunderstorm, J. Geophys. Res., 96: 12833–12855.